

# Polaronic signature in the metallic phase of $\text{La}_{0.7}\text{Ca}_{0.3}\text{MnO}_3$ films detected by scanning tunneling spectroscopy

S. Seiro,\* Y. Fasano, I. Maggio-Aprile, E. Koller, O. Kuffer, and Ø. Fischer  
*Département de Physique de la Matière Condensée, Université de Genève,*  
*24, Quai Ernest-Ansermet, 1211 Geneva, Switzerland*

(Dated: February 28, 2022)

In this work we map tunnel conductance curves with nanometric spatial resolution, tracking polaronic quasiparticle excitations when cooling across the insulator-to-metal transition in  $\text{La}_{0.7}\text{Ca}_{0.3}\text{MnO}_3$  films. In the insulating phase the spectral signature of polarons, a depletion of conductance at low bias flanked by peaks, is detected all over the scanned surface. These features are still observed at the transition and persist on cooling into the metallic phase. Polaron-binding-energy maps reveal that polarons are not confined to regions embedded in a highly-conducting matrix but are present over the whole field of view both above and below the transition temperature.

PACS numbers: 73.50.-h, 71.30.+h, 68.37.Ef

In manganite compounds such as  $\text{La}_{1-x}\text{Ca}_x\text{MnO}_3$  ( $0.2 < x < 0.5$ ), the coupling between lattice, magnetism and transport leads to a transition from metallic ( $d\rho/dT > 0$ ) to insulating ( $d\rho/dT < 0$ ) behavior in tune with the suppression of ferromagnetic order at a temperature  $T_{\text{MI}}$  [1, 2]. Understanding the transport properties of the insulating phase required the consideration of the electron-phonon coupling mechanism in addition to double-exchange interactions [3, 4]. In the strong coupling limit electrons are bound by a surrounding lattice distortion forming polaronic quasiparticles [3, 4]. In the insulating phase, polaron hopping is the dominant transport mechanism and gives rise to the measured thermally-activated resistivity [5, 6, 7]. Although in these context theoretical predictions [3, 4] state that on cooling below  $T_{\text{MI}}$  spin order leads to electron delocalization, evidence from numerous experimental techniques [8, 9, 10, 11, 12, 13] suggests the presence of polarons also at  $T < T_{\text{MI}}$ . Optical reflectivity [14] and structural [15, 16] investigations propose a crossover from a large to small-polaron regime on warming across the MIT and a coexistence of both polaronic phases at  $T \sim T_{\text{MI}}$ . Therefore, the existence of polarons in the metallic phase and the relevance of nanoscale inhomogeneities [2] to the metal-to-insulator transition (MIT) remain active subjects of debate. Insight into this problem can be gained from scanning tunnelling spectroscopy (STS) studies as the one presented here which probes local electronic properties at the atomic scale.

Although the phase separation scenario has gained popularity in recent years, it is mostly supported by results from macroscopic techniques [2]. Local spectroscopy studies in  $\text{La}_{1-x}\text{Ca}_x\text{MnO}_3$  claim electronic phase separation [17, 18, 19, 20], but a strong influence of chemical and structural disorder present in the samples cannot be ruled out. In contrast, a recent study in a fully-relaxed film reports homogeneous conductance maps [21].

However, conductance maps at a fixed energy do not provide enough information on the eventual presence, spectroscopic characteristics and spatial distribution of polaronic quasiparticles. Therefore, in this work we measure tunnel current vs. voltage maps with nanometric spatial resolution in  $\text{La}_{0.7}\text{Ca}_{0.3}\text{MnO}_3$  (LCMO) films, tracking polaronic quasiparticles when cooling across the MIT. The spectral signature of polarons is observed both above and below  $T_{\text{MI}}$  all over the field of view.

The LCMO film studied in this work was grown on a  $\text{SrTiO}_3$  substrate by RF sputtering at  $675^\circ\text{C}$ , in 0.2 Torr of a 50%Ar-50% $\text{O}_2$  mixture. Great effort was made to obtain a single-crystalline fully-strained film. By controlling strain  $T_{\text{MI}}$  can be reduced with respect to the bulk [22] allowing to access a wider temperature range of the insulating phase. The structure of 3D perovskites does not present an easy cleaving plane, so we thoroughly cleaned the surface of the film with isopropanol in an ultrasonic bath. The sample was immediately placed in the ultra-high vacuum chamber of a variable temperature home-made STS system [23], prior to cooling in  $^4\text{He}$  exchange gas. This procedure allowed us to obtain reproducible and high-quality topographic images as the one shown in Fig. 1. Topographs and current vs. voltage ( $I(V)$ ) maps were measured as a function of temperature, with particular detail in the range around  $T_{\text{MI}}$ . The tip, made of electrochemically etched Ir, was grounded and the bias voltage  $V$  was applied to the sample.

The thickness of the film, 31 nm, was obtained from x-ray reflectometry and confirmed by the Laue oscillations around the (002) reflection, which is shown in Fig. 1 (a). The  $c$  axis parameter was found to be  $(3.808 \pm 0.002)$  Å, 1.6% smaller than that of the bulk, as expected for tensile in-plane strain. The reciprocal space map in Fig. 1(b) shows that the in-plane lattice parameter matches that of  $\text{SrTiO}_3$ , i.e. the film is fully strained. The (103) pole figure in Fig. 1(c) shows that the film is single crystalline. The metal-to-insulator transition temperature,  $143.9 \pm 0.3$  K, was obtained from a four-point resistivity measurement, see Fig. 2, as the temperature where  $d\rho/dT$  changes sign. Topographs as the one in Fig. 1 (d)

\*Electronic address: silvia.seiro@physics.unige.ch

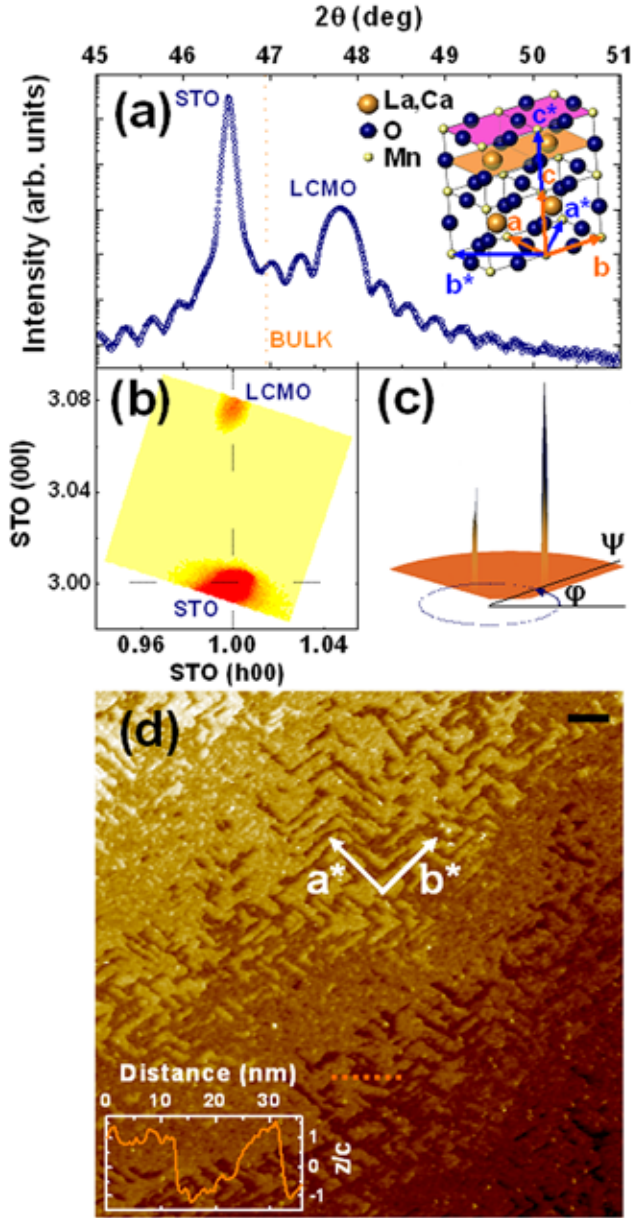


FIG. 1: (a) Main panel: X-ray diffractogram around the (002) pseudocubic reflection and size-effect oscillations. The film thickness was inferred to be 31 nm and the  $c$  axis parameter ( $3.808 \pm 0.002$ ) Å. Inset: Schematic crystalline structure. Pseudocubic ( $\mathbf{a}$ ,  $\mathbf{b}$ ,  $\mathbf{c}$ ) and orthorhombic ( $\mathbf{a}^*$ ,  $\mathbf{b}^*$ ,  $\mathbf{c}^*$ ) lattice vectors are indicated, as well as  $\text{MnO}_2$  (pink) and  $(\text{La,Ca})\text{O}$  (orange) planes. (b) Reciprocal space map around the (103) reflection. (c) Pole-figure measurement for the (103) direction. (d) Topograph measured in the constant-current mode with regulation conditions of 2 V and 0.4 nA at 144 K. The  $\mathbf{a}^*$  and  $\mathbf{b}^*$  vectors of the film are at  $45^\circ$  to the  $\mathbf{a}$  and  $\mathbf{b}$  axes of the substrate. The black scale bar represents 20 nm. The height profile in the insert corresponds to the dotted line (orange).

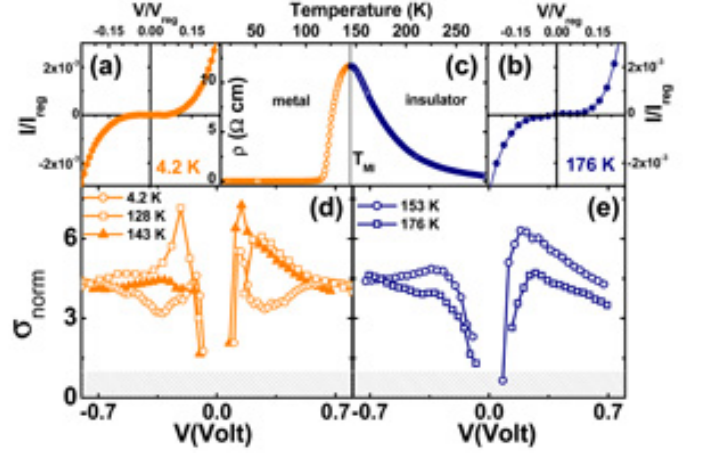


FIG. 2: Average tunneling  $I(V)$  curves for (a) 4.2 K (2 V/0.5 nA) and (b) 176 K (1.3 V/0.6 nA). (c) Macroscopic resistivity data:  $T_{\text{MI}} = 143.9$  K is indicated by a vertical line. (d) and (e) Selected normalized conductance curves at temperatures below and above  $T_{\text{MI}}$ , respectively. When the measured average current was below the experimental noise ( $\sim 10^{-2}$  pA) no estimation of  $\sigma_{\text{norm}}$  could be made (hatched regions).

reveal growth steps oriented along the  $\mathbf{a}^*$  and  $\mathbf{b}^*$  axis of the  $\text{La}_{0.7}\text{Ca}_{0.3}\text{MnO}_3$  orthorhombic structure. The height of steps is systematically a multiple of  $c$ , the pseudocubic lattice parameter, indicating the same terminating layer over the whole surface. Whether it is  $\text{MnO}_2$  or  $(\text{La,Ca})\text{O}$  planes could not be determined because, although rugosity was on average only 1 Å, atomic resolution [24] was not achieved. As we show in a previous report [25], local  $I(V)$  curves are not sensitive to the typical topographic features of our films and rather homogeneous at the nanoscale. Therefore the spatial average of  $I(V)$  curves is representative of spectroscopic properties over the whole sample surface.

In the STS experimental configuration, where a bias voltage  $V$  is applied between the sample and the tip, the differential conductance is given by

$$dI/dV \approx \frac{e^2}{\hbar} \rho_s(eV) \rho_t(0) T(eV, z), \quad (1)$$

where  $\rho_s(eV)$  is the sample density of states, the tip density of states  $\rho_t(0)$  is assumed to be constant and  $z$  is the tip-sample separation [26]. The latter is set by the junction impedance  $R_T = V_{\text{reg}}/I_{\text{reg}}$ , that in STS experiments is typically 1 GΩ. If an electron is bound in a polaron, the process of an electron tunnelling into the tip requires the unbinding of the quasiparticle, with an energy cost of  $E_b$ . As a consequence, STS probes the local spectrum of the quasiparticles resulting from the unbinding of polarons.

For bias voltages much smaller than the barrier height  $\phi$ , the tunnel transmission coefficient  $T$  does not depend on  $V$  and the measured differential conductance is proportional to  $\rho_s(eV)$ . At voltages that are a non-negligible fraction of  $\phi$ , as in the case of the measurements pre-

sented here, the tunnel coefficient can no longer be considered voltage-independent. For moderate voltages an adequate estimation of  $T(eV, z)$  is given by  $I/V$  [26]. Therefore, the numerically derived  $I(V)$  curves were normalized to obtain  $\sigma_{\text{norm}} = (dI/dV)/(I/V) \propto \rho_s(eV)$ , the normalized conductance. At  $V \sim 0$ , the noise on the tunnel current hinders an appropriate estimation of  $T(eV, z)$  with  $I/V$ . As a consequence, at low voltages,  $T(eV, z)$  was estimated with a WKB-like tunnel transmission coefficient [27].

In this work  $10^4$  single  $I(V)$  curves were spatially averaged over  $60 \times 60 \text{ nm}^2$ . Examples of average  $I(V)$  curves in the metallic and insulating phases are shown in Fig. 2. At all measured temperatures  $dI/dV$  at zero bias is below the experimental resolution of typically  $10^{-4} \text{ nS}$ . In the high-temperature phase  $\sigma_{\text{norm}}$  presents a depletion around the Fermi level flanked by conductance peaks, as shown in Fig. 2 (c). These features are the spectral signature of polarons and the half-distance between the peaks,  $\Delta_B$ , is a measure of the polaron binding energy [12]. At 176 K, well above  $T_{\text{MI}}$ ,  $\Delta_B = (0.30 \pm 0.07) \text{ eV}$  is consistent with the polaron binding energy obtained by fitting the high-temperature resistivity data with an adiabatic small-polaron model, see Fig. 3. Within this model  $\rho = \rho_0 T \exp(E_A/kT)$  [5] and the binding energy can be estimated as  $E_b \approx 2E_A = (0.24 \pm 0.02) \text{ eV}$  [5].

In the metallic phase these polaronic characteristics persist even down to 4.2 K, see Fig. 2 (d). Although in contrast to the theoretical prediction that polarons disappear below  $T_{\text{MI}}$  [3, 4], our local spectroscopic results are consistent with data from different experimental techniques [8, 9, 10, 11, 12, 28]. On decreasing temperature  $\Delta_B$  globally shifts to lower energies, as shown in Fig. 3. This behavior is consistent with the temperature evolution of polaron binding energies obtained from macroscopic optical reflectivity data [28]. In spite of all these evidence, the role of polarons in the transport properties of the metallic phase is currently under discussion [29, 30].

Remarkably, on top of the global temperature behavior,  $\Delta_B$  presents a dip at  $T_{\text{MI}}$ . Although STS probes the quasiparticle spectrum at the surface, the extreme sensitivity of  $\Delta_B$  to the MIT and its quantitative agreement with the  $E_b$  estimated from transport data indicate that the  $\sigma_{\text{norm}}$  measured in this work is representative of bulk properties.

Since normalized conductance curves in Fig. 2 come from a spatial average of  $10^4$  curves, it could be argued that the polaronic signal observed below  $T_{\text{MI}}$  comes from remnant domains of the high-temperature phase. Polaron-binding-energy maps reveal that this is not the case: The spectroscopic signature of polarons is detected over the whole field of view of  $60 \times 60 \text{ nm}^2$  with a spatial resolution of  $\sim 2$  unit cells. The binding-energy distributions are Gaussian with a dispersion of up to 20% which does not significantly change with temperature (it varies only 2.5% from 176 to 140 K). No bimodal distribution of  $\Delta_B$  is detected within 0.03 eV, a resolution which is of

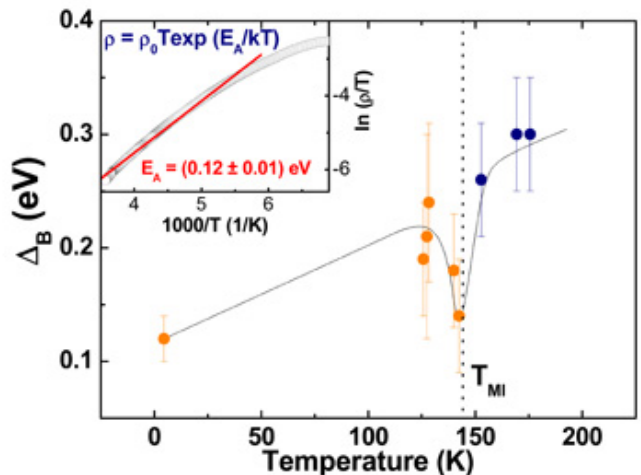


FIG. 3: Temperature dependence of the polaron binding energy estimated from normalized conductance curves as half the peak-to-peak separation. The dotted line is a guide to the eye. Inset: Fit (red line) of the high-temperature resistivity data (open symbols) with a small-polaron adiabatic model (see text).

the order of the thermal energy.

At low temperatures, the non-linear dependence of  $I$  on the bias voltage might seem in contradiction with a metallic state. This striking result can have different origins. Firstly, in order to probe polarons spectroscopy has to be performed in the energy scale of  $E_b$ , which is a non-negligible fraction of  $\phi$ . As a consequence, the tip-sample separation is large and simultaneously, the transmission coefficient increases with voltage, resulting in a non-linear  $I(V)$  characteristic. Secondly, the macroscopic resistivity of the 31 nm film has a value of  $4 \text{ m}\Omega \text{ cm}$  at 4.2 K, 3 orders of magnitude larger than for a common metal, implying that the number of carriers and/or their mobility is low. Recent angle-resolved photoemission spectroscopy (ARPES) measurements in the bilayer manganite  $\text{La}_{1.4}\text{Sr}_{1.6}\text{Mn}_2\text{O}_7$ , revealed the presence of “nodal” quasiparticles that would account for the poor conductivity of the metallic phase [30]. Since the measured tunnel current comes from a reciprocal-space integration of the single particle spectral function (as detected by ARPES) [31], the contribution to the tunnel conductance at  $E_F$  will be extremely small. Therefore, a low tunnel conductance at zero bias is not at odds with metallic behavior. In addition to the measurements presented in this work, previous STS studies report highly nonlinear spectra in the metallic phase of a  $\text{La}_{0.7}\text{Ca}_{0.3}\text{MnO}_3$  film at 77 K [12] and in a cleaved  $\text{La}_{1.4}\text{Sr}_{1.6}\text{Mn}_2\text{O}_7$  crystal [13]. In order to study the spectral features close to the Fermi level, high energy-resolution measurements at small  $z$  are currently underway and will be the subject of a future report. We stress that this work focuses on the temperature evolution and spatial homogeneity of polaronic spectral features that are manifest at an energy scale of  $\sim 0.1 - 1 \text{ eV}$ .

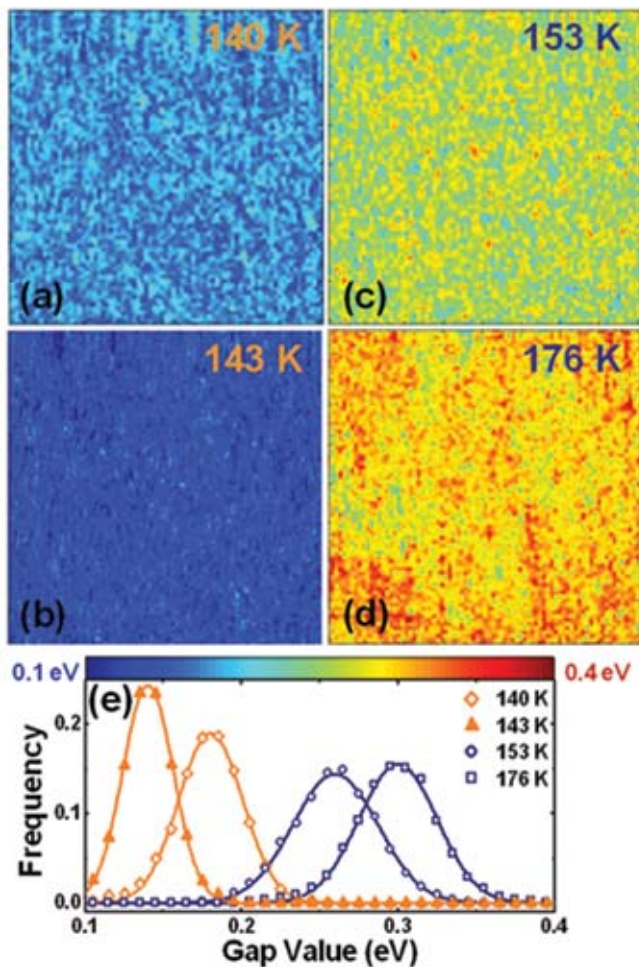


FIG. 4: Mapping of local  $\Delta_B$  values at (a) 140, (b) 143, (c) 153 and (d) 176 K. All maps correspond to  $60 \times 60 \text{ nm}^2$  areas with a resolution of  $7.5 \text{ \AA}/\text{pixel}$ . (e) Distributions of  $\Delta_B$  values (symbols) obtained from the maps fitted with a Gaussian law (lines). The average noise of local  $I(V)$  curves in all maps is comparable, ranging from 0.2 to 0.4 pA.

In summary, we present tunneling spectroscopic evidence for the presence of polarons in the insulating phase and their persistence on cooling through the insulator-to-metal transition down to 4.2 K. The spectroscopic signature of polarons is detected over the whole field of view at all measured temperatures. This novel result brings forth the challenge of understanding the role played by polaronic quasiparticles in the metallic phase of manganites.

#### Acknowledgments

This work was supported by the Swiss National Science Foundation and the MaNEP program of the Swiss National Center of Competence in Research.

- 
- [1] *Colossal magnetoresistive oxides*, edited by Y. Tokura, Advances in Condensed Matter Science Vol. 2 (Gordon and Breach, Amsterdam, 2000).
- [2] E. Dagotto, *Nanoscale Phase Separation and Colossal Magnetoresistance* (Springer-Verlag, Berlin, 2003).
- [3] A. J. Millis, P. B. Littlewood, and B. I. Shraiman, Phys. Rev. Lett. **74**, 5144 (1995).
- [4] A. J. Millis, B. I. Shraiman, and R. Mueller, Phys. Rev. Lett. **77**, 175 (1996).
- [5] D. C. Worledge *et al.*, J. Appl. Phys. **80**, 5158 (1996).
- [6] M. Jaime *et al.*, Phys. Rev. B **54**, 11914 (1996).
- [7] J. M. De Teresa *et al.*, Nature **386**, 256 (1997).
- [8] M. F. Hundley *et al.*, Appl. Phys. Lett. **67**, 860 (1995).
- [9] A. S. Alexandrov *et al.*, Phys. Rev. B **64**, 140404(R) (2001).
- [10] G.-M. Zhao, V. Smolyaninova, W. Prellier, and H. Keller, Phys. Rev. Lett. **84**, 6086 (2000).
- [11] M. Quijada *et al.*, Phys. Rev. B **58**, 16093 (1998).
- [12] J. Y. T. Wei, N. C. Yeh, and R. P. Vasquez, Phys. Rev. Lett. **79**, 5150 (1997).
- [13] H. M. Rønnow *et al.*, Nature **440**, 1025 (2006).
- [14] S. Yoon *et al.*, Phys. Rev. B **58**, 2795 (1998).
- [15] D. Louca *et al.*, Phys. Rev. B **56**, R8475 (1997).
- [16] A. Lanzara *et al.*, Phys. Rev. Lett. **81**, 878 (1997).
- [17] M. Fäth *et al.*, Science **285**, 1540 (1999). Sample characterization is described in S. Freisem *et al.*, J. Magn. Magn. Mater. **165**, 380 (1997).
- [18] T. Becker *et al.*, Phys. Rev. Lett. **89**, 237203 (2002).
- [19] S. F. Chen *et al.*, Appl. Phys. Lett. **82**, 1242 (2003).
- [20] V. Moshnyaga, L. Sudheendra, O. I. Lebedev, S. A. Köster, K. Gehrke, O. Shapoval, A. Belenchuk, B. Damaschke, G. van Tendeloo, K. Samwer, Phys. Rev. Lett. **97**, 107205 (2006).
- [21] J. Mitra *et al.*, Phys. Rev. B **71**, 094426 (2005).
- [22] X. F. Song, G. J. Lian and G. C. Xiong, Phys. Rev. B **71**, 214427 (2005).

- [23] A. D. Kent *et al.*, *Ultramicroscopy* **42-44**, 1632 (1992).
- [24] To our knowledge, atomic resolution on manganite films has only been recently achieved and reported in J. X. Ma, D. T. Gillaspie, E. W. Plummer, and J. Shen, *Phys. Rev. Lett.* **95**, 237210 (2005).
- [25] S. Seiro, Y. Fasano, I. Maggio-Aprile, O. Kuffer and Ø. Fischer, *J. Magn. Magn. Mater.*, **310**, 243 (2006).
- [26] P. Mårtensson and R. M. Feenstra, *Phys. Rev. B.* **39**, 7744 (1989).
- [27] V. A. Ukraintsev, *Phys. Rev. B.* **53**, 11176 (1996).
- [28] C. Hartinger, *et al.*, *Phys. Rev. B* **69**, 100403(R) (2004).
- [29] Guo-meng Zhao, H. Keller and W. Prellier, *J. Phys.: Condens. Matter* **12**, L361 (2000).
- [30] N. Mannella *et al.*, *Nature* **438**, 474 (2005).
- [31] Ø. Fischer, M. Kugler, I. Maggio-Aprile, C. Berthod, Ch. Renner. *Rev. Mod. Phys* **79**, 353 (2007).